J. Comput. Appl. Res. Mech. Eng. Vol. 13. No. 1, pp. 1-12, 2023 *DOI: 10.22061/JCARME.2023.9491.2273*

Journal of Computational and Applied Research in Mechanical Engineering

jcarme.sru.ac.ir

SRTTU

JCARME

ISSN: 2228-7922

Research paper

Numerical simulation of extracorporeal membrane oxygenators to investigate important parameters and membrane thickness in oxygen exchange rate

Behnam Dilmaghani Hassanlouei[a] , Nader Pourmahmoud[a,*] and Pierre Sullivan[b]

[a]*Department of Mechanical Engineering, Faculty of Engineering, Urmia University, Urmia, Iran*
[b]*Department of Mechanical and Industrial Engineering, University of Toronto, Toronto, M5S 3G8, Canada*

Article info:

Article history:

Received: 15/12/2022

Revised: 26/06/2023

Accepted: 30/03/2023

Online: 03/04/2023

Keywords:

Microfluidic blood oxygenator,

Extracorporeal membrane oxygenation,

Computational fluid dynamics,

Porous media,

Polydimethylsiloxane membrane.

[*]Corresponding author:
n.pormahmod@urmia.ac.ir

Abstract

In this article, an extracorporeal membrane oxygenator (ECMO) is simulated in 2D geometry using computational fluid dynamics (CFD). Momentum and mass transport equations were solved for the laminar flow regime ($30 < Re < 130$ for the blood channel) using the finite element method. In this study, the software COMSOL was used as the solver. To this end, the main problem of ECMO devices is the pressure drop and the risk of thrombus formation due to blood stagnation, so to solve this problem, the oxygen transfer rate to blood should be increased. Therefore, to optimize the oxygen transfer rate of blood, three basic parameters were examined: blood flow velocity, oxygen velocity, and membrane thickness. Blood flow was considered at five different velocities (0.2, 0.4, 0.5, 0.6, and 0.8 mm/s). Results showed that increased blood flow velocity adversely affected oxygen permeability, increasing oxygen permeability from about 60% at 0.2 mm/s to about 24% at 0.9 mm/s. In addition, five different membrane thicknesses (0.04, 0.06, 0.08, 0.2, and 0.3 mm) were investigated, and, as expected, better oxygen exchange occurred as the membrane thickness decreased. We also found that the diffusion rate is about 40% for the 0.4 mm/s thin films and about 25% for the same inlet velocity and larger film thickness. Furthermore, the oxygen diffusivity increases from 28% to 38% as the oxygen gas velocity increases. However, oxygen velocities above 0.8 mm/s should not be used, as the range of oxygen diffusivity variation decreases with higher oxygen gas velocities.

1. Introduction

A method for treating patients with severe respiratory failure is artificial respiration for the patient using mechanical ventilation. However, the ventilator is not sufficient for acute respiratory patients in some cases. One of the alternative treatments is the use of membrane blood oxygenators (MBOs), which usually refers to extracorporeal membrane oxygenation (ECMO) [1, 2]. While the ECMO device for severe respiratory patients can be an essential rescue device, clinical use is limited due to the high risks of complications. However, the

success of the Conventional ventilatory support vs. Extracorporeal membrane oxygenation for Severe Adult Respiratory failure (CESAR) study and the emergence of type the flu (H1N1) in 2006 and 2009 respectively, resulted in an increase in the use of ECMO devices in patients [3, 4].

Scientists study ECMO devices and factors affecting the oxygen uptake rate, trying to improve the exchange of oxygen with the blood. Accordingly, experimental or numerical works can be used to study these devices and predict oxygen exchange rates. Still, since practical work is much more expensive than numerical simulation, researchers are more inclined to use numerical simulation. By mathematically modeling the oxygen transfer rate in hollow fiber membrane oxygen generators can predict the rate of oxygen transfer well [5, 6]. In this modeling, they used the term "Effective diffusivity" instead of molecular diffusion of oxygen for absorption by blood hemoglobin. Catapano *et al.* [7] proposed a porous medium model to predict the behavior of hollow fiber membranes; in this method, they show that making hollow membranes behave like a porous medium is acceptable. In ECMO's 70 years of evolution, the membrane of ECMO systems has gone through three generations, from a PDMS flat membrane to a hollow fiber membrane [8]. Evren [9] also used the convection-diffusion equation to model the gas transfer of oxygen to water in micro-porous polypropylene membranes and showed that using these equations would produce acceptable results for predicting the rate of oxygen exchange to water; however, the processes involved in the uptake of oxygen by hemoglobin were not modeled. Zhang *et al.* [10] used the computational fluid dynamics (CFD) method to predict oxygen exchange rates in hollow fiber membrane-based oxygen generators to solve blood flow and mass transfer equations in which oxygenation of the blood is considered as a convection-diffusion process and the hollow fiber membrane bed is considered as a porous medium. Comparing the results obtained from the CFD method with the experimental results obtained from the commercial Medtronic Affinity NT blood-gas oxygenator, showed that computational fluid dynamics can be used to predict the flow field, pressure distribution, and oxygen transfer in oxygen generators.

The membrane of most oxygen generators is based on hollow fibers as the basic unit of gas exchange [10]. Hollow fiber-based oxygen generators were originally designed to allow blood to flow through the hollow fibers and the exchanged gas to penetrate them through an enclosed sheath [11]. In these devices, due to the high resistance to flow and shear friction caused by blood, the pressure is high to deal with these forces and proper blood circulation. The device needs a pump, which increases the possibility of hemolysis and thrombotic reaction [11, 12]. Changes in the configuration of this type of device significantly reduce the pressure drop but increase the initial volume (Priming volume) and, ultimately, reduce the efficiency of gas exchange, which makes the device unsuitable for short-term and premature infants [13-17]. In addition, blood flow is not uniform in this configuration, and stagnant areas, secondary flows, and high incision areas may be present, leading to high levels of heparin to dilute the blood, with risks and complications for the patient. Understanding these limitations, microfluidic devices have been developed to create a smoother and more uniform blood flow in the vicinity of the gas exchange membrane with optimum pressure drop, low initial volume, and suitable gas exchange capability [18, 19]. ECMO microfluidic devices attempt to mimic one or more features of the main gas exchange interface of the lung tissue. The high surface-to-blood ratio (300 cm per meter), its low thickness (1 to 2 μm), and the small size of the perfusion channels in the blood lead to high permeability in gases. In these microfluidic devices, the membrane is usually polydimethylsiloxane (PDMS) [20-26]. Dabbaghi *et al.* [27] introduced a new concept in which a closed gas holding chamber is created on either side of the blood channel called the four-side microfluidic blood oxygenator (fsMBO). They also demonstrated that the performance of such devices was superior to that of the equivalent double-side microfluidic blood oxygenator (dsMBO). They showed that such a design would increase the gas exchange level without

affecting the channel's geometry or flow characteristics. By examining the impact of the ECMO device's capillary channel height at three different heights (30, 60, and 100 micrometers), Lindsay *et al.* [28] concluded that while the pressure drop and gas exchange are nearly identical for all three designs, the capillary channel with a height of 60 micrometers had a higher wall shear rate. Dong Han *et al.* created a new portable ECMO system to make it easier for patients receiving ECMO support to move around since they must use the ECMO equipment continually [29].

Due to the advantages and disadvantages of different types of ECMO and blood oxygenators, the use of microfluidic systems has increased recently. In this study, the process of oxygen exchange with blood, a disposable microfluidic ECMO system with three channels for blood, membrane, and oxygen gas was investigated. This study examines the effects of essential parameters such as blood flow velocity, oxygen gas velocity, and membrane thickness. First, various velocities are considered to examine the effect of blood flow velocity on the oxygen diffusion rate into blood channels. Then, five different film thicknesses are investigated to check the amount of oxygen exchange at different film thicknesses. Finally, the effect of oxygen gas velocity on the diffusivity into blood channels was examined to optimize this phenomenon. The results of this study will help improve the efficiency of membrane oxygen exchange systems.

2. The ECMO model description

The patient's venous blood or deoxygenated blood, is removed with a catheter from the patient's right atrium and passes through the ECMO cycle [1]. The blood is pumped and mixed with other fluids such as heparin (Heparin is an anticoagulant (blood thinner) that prevents the formation of blood clots), if needed. A membrane (gray channel) separates two compartments (Fig. 1): one for the deoxygenated blood (red channel), and the other for sweeping gas (blue channel). Oxygen in the gas penetrates through the membrane's pores and enters a fluid boundary layer close to the membrane surface. The oxygen boundary layer formed near the surface of the membrane, which contains more oxygen, reduces the pressure gradient of oxygen in the membranes of the ECMO device, thereby reducing the oxygen flux of the membrane. Finally, after crossing a boundary layer, it penetrates a large part of the plasma by the diffusion mechanism, where it can be transported to red blood cells by hemoglobin.

The physical and stationary parameters used in the oxygen exchange simulation in the ECMO system are given in Table 1.

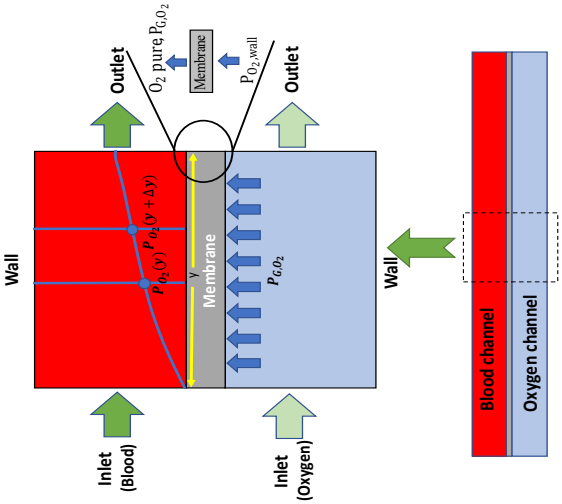

Fig. 1. Schematic of the thematic geometry studied in the present study, the boundary conditions, and the one-way transmission system.

Table 1. The main blood and oxygen-related constant parameters.

Parameter	Symbol	Value
Solubility coefficient of O_2 in plasma [10]	a	9.37×10^{-4} $(mol\, m^{-3} mbar^{-1})$
Diffusion coefficient of O_2 [10]	D_b	1.8×10^{-9} $(m^2 s^{-1})$
Number of binding sites of Hb [30]	n	2,85
Partial pressure of O_2 at 50% blood saturation [30]	P_{50}	38.7 $(mbar)$
O_2 density	d	1331 (gm^{-3})
Blood density [10]	ρ	1050 (kgm^{-3})
Blood viscosity [10]	μ	2.9×10^{-5} $(mbar\, s)$

In the present study, the issue of oxygen diffusivity through the membrane process into the blood channel is considered, and we examined parameters such as gas and blood inlet velocity as well as membrane thickness that can have a significant impact on the performance of the ECMO system. Fig. 1 is a schematic of the geometry studied.

3. Numerical model of ECMO systems

3.1. Governing equation and boundary conditions

Flow distribution in blood and gas microchannels was numerically solved in 2D using COMSOL Multiphysics (version 5.6) Software and adapted to describe the flow along the microchannel, a laminar flow regime for blood and oxygen gas channel was adapted (Reynolds numbers are between 30 and 130). The momentum equation for the laminar flow regime is solved simultaneously with the mass equation. The following is the Navier-Stokes equation:

$$\rho(u.\nabla)u = [-pI + \mu(\nabla u + (\nabla u)^T) - \frac{2}{3}\mu(\nabla.u)I] \quad (1)$$

$$\nabla.(\rho u) = 0 \quad (2)$$

where ρ represents the blood density, u stands for the flow velocity vector field, p represents the pressure, μ represents the blood viscosity, and T represents the matrix transposition. In Eq. (1), the left side represents the acceleration forces and the right side represents the pressure gradient and the adhesive forces. The following assumptions are also considered in these equations: simulation is steady, blood and gas flow are assumed to be incompressible, non-slip condition in the walls of the blood chamber; $u = 0$, there is no reverse -flow, the direction of flow is perpendicular to the inlet plates and the outlet pressure is set to 1 atmosphere.

The set of governing equations was solved using the finite element method. The convergence criterion is based on the residual error in the motion equation, which was set to 10^{-3}.

Furthermore, as shown in Fig. 2, the geometry consists of three rectangular channels, from left to right, blood channel, membrane channel, and gas channel, respectively. Also, each airway and blood way has an entrance and an exit, and each has a wall. Channel dimensions and sizes are shown in Table 2.

3.2. Oxygen transport model

The general mass transport equation was developed from the standard convection-diffusion mass transport equation to model these prosses [21, 23, 31]. The partial differential equation of oxygen transfer in the blood and the steady state condition can be written as follows [32]:

$$u.\nabla P_{O_2} = D_{eff}.\nabla^2 P_{O_2} \quad (3)$$

D_{eff} indicates the effective diffusivity of oxygen into the bloodstream, which includes the effects of oxygen uptake by hemoglobin and is first introduced by Mocros and Leonard [31] D_{eff} is:

$$D_{eff} = \frac{D_b}{1+\lambda(P)} \quad (4)$$

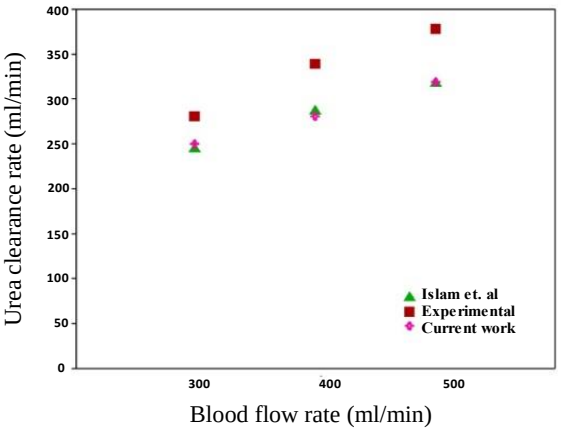

Fig. 2. Comparison of the proposed model with the results of the numerical solution and the experimental data.

Table 2. Channel dimensions.

Height of the channel	Width of the blood and air channel	Membrane thickness
21 mm	0.4 mm	0.04 -0.3 mm

In Eq. (4), D_b is the oxygen diffusion coefficient in plasma, $\lambda(P)$ a mathematical equation developed to calculate the oxygen concentration in blood hemoglobin, denoted by $[Hb]$. This relationship is defined according to Eq. (5), which is as follows. In this equation, $\lambda(P)$ represents the concentration of oxygen in plasma:

$$\lambda(P) = \frac{1.34[Hb].S'_{O_2}}{\alpha} \quad (5)$$

And also, for S'_{O_2} we have:

$$S'_{O_2} = \frac{n(P_{50})^n P_{O_2}{}^{n-1}}{(P_{50}{}^n + P_{O_2}{}^n)^2} \quad (6)$$

And from Hill's equation, we have [10, 33]:

$$S_{O_2} = \frac{(P_{O_2}/P_{50})^n}{1+(P_{O_2}/P_{50})^n} \quad (7)$$

where S_{O_2} is the oxygen saturation concentration, n is the number of hemoglobin binding sites known as the Hill coefficient, and P_{50} is the partial pressure of oxygen when it is at 50% of its saturation state. The parameter n is the Hill's equation for a specific blood type. By matching the experimental data [10] at saturation state with the Hill curve, $n = 2.84$, and $P_{50} = 38.7$ mbar was obtained. The parameter P_{50} depends on temperature, T, and pH, which is expressed as follows for cow blood [31]:

$$P_{50} = 38{,}75\times10^{(-0{,}41)(7{,}4-pH)}\times10^{(-0{,}024)(37-T)} \quad (8)$$

Combining Eqs. (4 and 8), the effective influence of D_{eff} is:

$$D_{eff} = \frac{D_b}{1+\frac{1.34[Hb].n(P_{50})^n.P_{O_2}{}^{n-1}}{\alpha(P_{50}{}^n + P_{O_2}{}^n)^2}} \quad (9)$$

By coupling the oxygen mass balance in the plasma and the membrane surface, boundary conditions are obtained to solve the mass transfer equation. The oxygen flux in the boundary condition is equal to the amount of oxygen diffusivity in the PDMS membrane layer as follows [30]:

$$J_{O_2} = D_m.a_m.(P_{G,O} - P_{O_2,wall}).\frac{1}{t_m} \quad (10)$$

where D_m represents the diffusion coefficient of oxygen in the membrane, a_m is the solubility of oxygen in the membrane, t_m is the thickness of the membrane layer, $P_{O_2.wall}$ is the partial pressure of oxygen in the thin film wall and P_{G,O_2} represents the partial pressure of oxygen in the gas channel. The two parameters D_m and a_m are related to the permeability of the membrane.

Overcoming the resistance of the boundary layer on the blood side is a significant challenge in the development of oxygenators. To prevent fluid turbulence and thrombosis, most oxygen generators are designed to operate in laminar flow regimes. Based on the Blasius solution for the laminar boundary layer equations, the relationship between the thickness of the boundary layer (δ) along the membrane surface in position x and the Reynolds number is as follows [34]:

$$\delta \approx \frac{4.9x}{\sqrt{\mathrm{Re}_x}} \quad (11)$$

3.3. Problem validation

To validate the proposed model and compare them with previous works, the effect of urea depletion rate on the inflow of blood flow was presented by Islam *et al.* [35] and also, with the experimental results provided by the manufacturer [35] (Fig. 2). The results were obtained by varying the blood flow rate while maintaining all other conditions constant as are depicted in Fig. 2.

There is an acceptable correlation between the results obtained, with the maximum error against the experimental method data being approximately 15% and the maximum error

against the numerical solution being approximately 3%.

3.4. Mesh independence study

The governing equations and related boundary conditions from above are solved numerically using the finite element method using COMSOL Multiphysics (version 5.6). As shown in Fig. 3(a) quadrilateral grid is used for meshing. A coarser mesh is used in the blood and oxygen gas channel than in the membrane thickness channel. Four different meshes (25105, 46400, 48720, 52200, and 105000) were investigated. According to the results of Fig. 3(b), the network with 48720 cells has been selected as a suitable computational network because by increasing the number of cells from 48720 to 105000, the oxygen concentration profile does not appreciably change. Therefore, to prevent the increase of computational volume and reduce the solution time, the network with the mentioned number of cells has been used. Table 3 shows some mesh quality indicators including skewness.

4. Results and discussion

4.1. The effect of different blood velocity

Blood flow velocity can have a significant effect on increasing the diffusivity of oxygen in the blood channel of ECMO systems. Therefore, we examined blood flow in five velocities, including 0.2, 0.4, 0.5, 0.6, and 0.8 mm/s. The oxygen concentration profiles at the outlets of the gas channels, membranes, and blood channels at different blood inlet velocities are given in Fig. 4(a). In Fig. 4(a), which shows the oxygen concentration profile at the exit of the blood channel, it is clear that as the velocity decreases, more oxygen enters the blood. Still, as the blood velocity increased, the oxygen could enter the blood channel with greater slope and velocity.
The concentrations of blood, membrane, and oxygen channels are all shown in this figure, as well. Also, the percentage of oxygen diffusivity in the blood channel is shown in Fig. 4(b), which shows the rate of oxygen diffusivity from the gas channel to the blood channel.

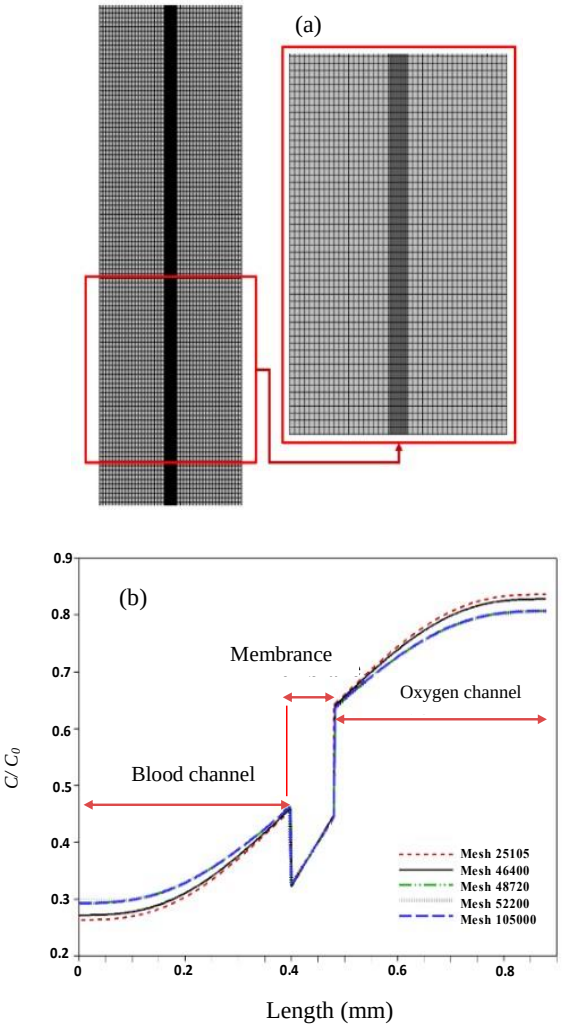

Fig. 3. (a) Grid geometry with a number of 48720 elements and (b) the oxygen concentration profiles at the outlet of blood, membrane, and gas channels for four different meshes.

Table 3. Number of elements in channel and skewness

Number of elements		Number of elements	
48720		10500	
Number of elements in membrane	15120	Number of elements in membrane	30000
Skewness in membrane	0.31	Skewness in membrane	0.34
Number of elements in channels	33600	Number of elements in channels	75000
Skewness channels	0.842	Skewness channels	0.875

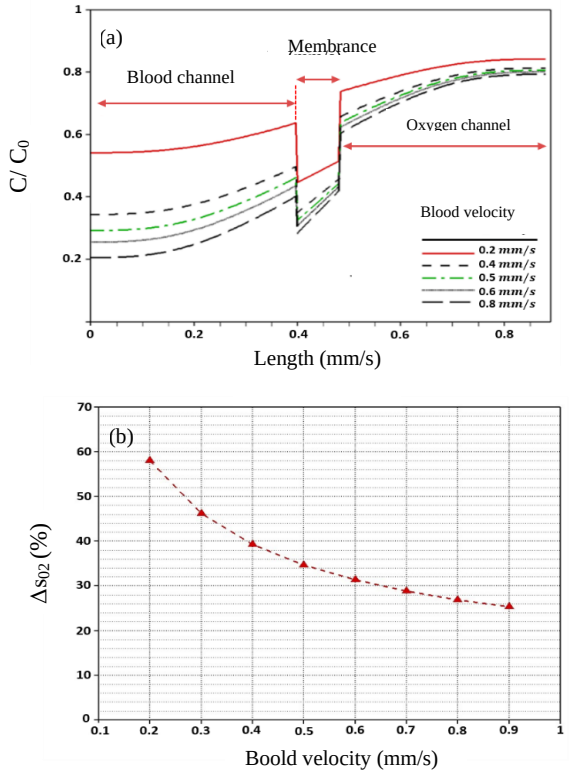

Fig. 4. (a) The oxygen concentration profile at the outlet of blood, membrane, and gas channels and (b) indicates the percentage of oxygen diffusivity into the bloodstream.

According to the presented results, an increase in the velocity of blood entry has a negative effect on oxygen diffusivity, so at velocities of 0.8 and 0.9 mm/s, the percentage of oxygen diffusivity is 26% and 24%, respectively.

However, the highest oxygen efficiency was observed at lower blood flow rates, so the oxygen diffusivity percentage reached 60%. Also, to show better results and compare the distribution of oxygen concentration along the channels, concentration contours at three blood flow velocities of 0.2, 0.5, and 0.9 mm/s are shown in Fig. 5. As is clear from this figure, by reducing the blood flow velocity, oxygen has the opportunity to permeate the boundary layer formed near the membrane into the blood, which is not possible at high velocity.

As shown in Fig. 4, as blood velocity decreases, there is more chance for oxygen exchange between the blood channel and the oxygen channel, and it leads to better oxygen exchange. At first, O_2 enters a fluid boundary layer close to the membrane surface, and in these areas, viscous forces are more dominant than convection forces.

In the case of O_2, the oxygen boundary layer near the membrane surface (which contains more oxygen) reduces the oxygen pressure gradient in the ECMO membranes, thereby reducing the O_2 membrane flux. In the next step, O_2 is diffused from the boundary layer and reaches most of the flowing plasma, and is finally absorbed by the hemoglobin in the red blood cells.

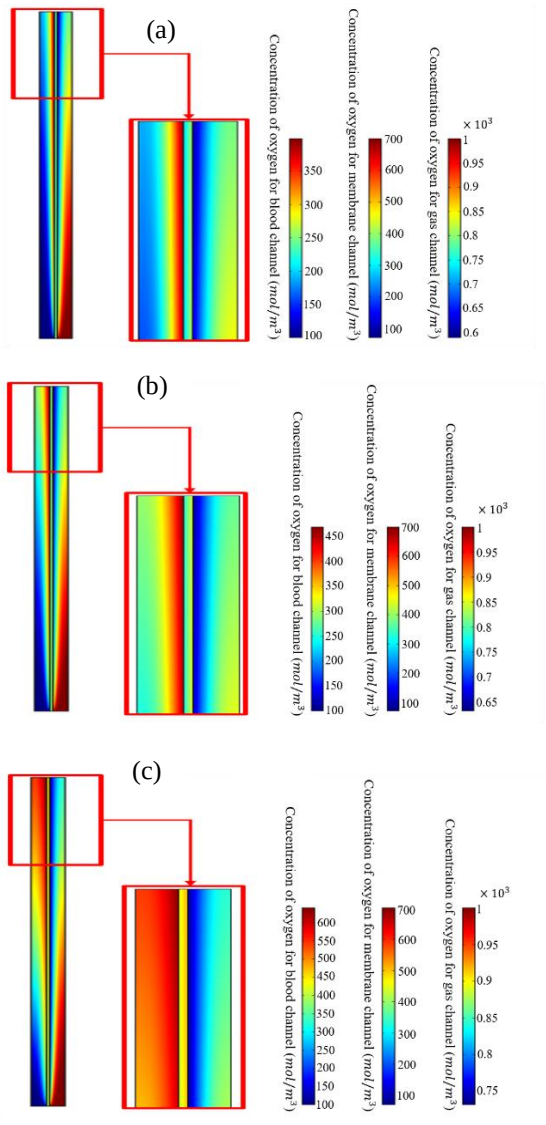

Fig. 5. The oxygen concentration contour along three channels of blood, membrane, and gas at three different inlet velocities; (a) 0.9 mm/s, (b) 0.5 mm/s, and (c) 0.2 mm/s.

Most of the resistance to oxygen diffusivity into the bloodstream is due to the oxygen boundary layer formed near the membrane in the bloodstream. [12, 36, 37]. From Eq. (11), we know that the thickness of the boundary layer has a reverse relation with blood velocity, meaning that higher blood flow velocities reduce the thickness of the boundary layer and make oxygen exchange more efficient. In the present study, as blood and oxygen gas both enter from one side, by increasing blood velocity, the blood has less opportunity to exchange oxygen with the oxygen channel and therefore reduces the percentage of oxygen diffusivity in the blood channel (Fig. 4(b)). However, as shown in Fig. 4(b), as the velocity of the blood increases, the rate of the changes in the percentage of oxygen diffusivity into the bloodstream decreases. This is due to the resistance of the boundary layer, which falls at high velocities of the boundary layer and makes the gas exchange more efficient. As can be seen from Fig. 5, one of the key parameters of oxygen permeability is the permeation resistance of this layer, by increasing the blood flow velocity the thickness of the boundary layer near the membrane reduces, making permeation more efficient.

4.2. The effect of different membrane thickness

At a constant rate of blood and gas inflow, the percentage of oxygen diffusivity for different membrane thicknesses (0.04, 0.06, 0.08, 0.2, and 0.3 mm) was studied. However, it was expected that a decrease in membrane thickness due to a decrease in oxygen concentration resistance would result in a higher percentage of oxygen diffusivity. At the blood and gas inlet velocity of 0.4 mm/s, the oxygen concentration profiles at the channel outlet and the oxygen diffusivity percentage are presented in Fig. 6. As expected, at lower membrane thickness or significantly thinner thickness (0.04 mm) due to reduced membrane diffusivity resistance, the percentage of oxygen diffusivity was higher about 40% (Fig. 6(b)). The concentration contour along the channels and membranes is shown in Fig. 7 for three different thicknesses, and the difference in the percentage of oxygen in the blood channel is shown qualitatively.

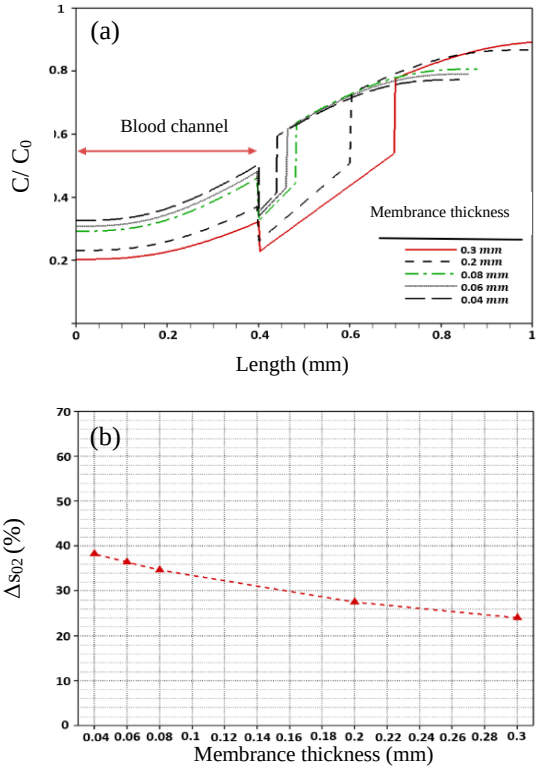

Fig. 6. (a) The oxygen concentration profile at the outlet of blood, membrane, and gas channels for membranes of different thicknesses and (b) a percentage of oxygen diffusivity into the bloodstream relative to membrane thickness

As can be seen in this figure, better oxygen permeation occurs as the membrane thickness decreases. To determine the concentration of oxygen in the three channels of blood, membrane, and oxygen, three types of column coloring are used, which are related to the blood channel, membrane, and oxygen channel, from left to right, respectively.

4.3 The effect of different gas velocity

The gas flow rate varies from 0.2 mm/s to 0.8 mm/s, while the blood flow velocity remains constant (0.4 mm/s), thereby increasing the amount of oxygen entering the channel. The increase in oxygen gas flux is proportional to the increase in oxygen concentration across the membrane.

As the oxygen gas flow rate increases, the concentration gradient across the film also increases, as shown in Fig. 8(a).

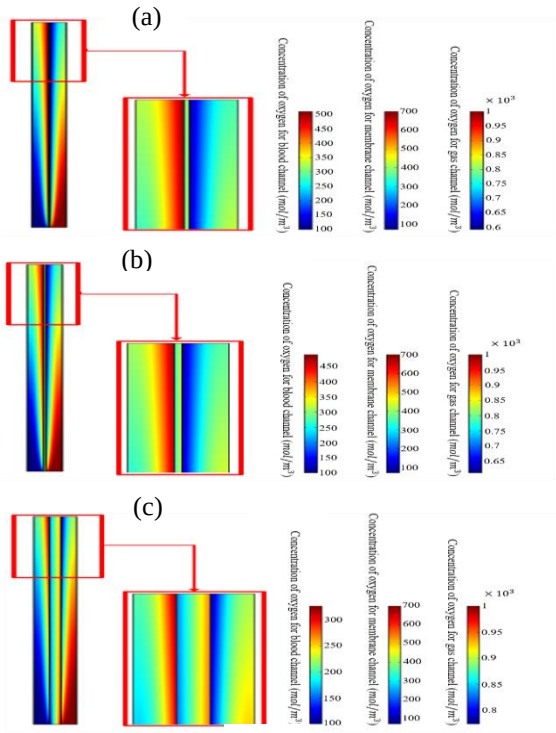

Fig. 7. The oxygen concentration contour along three channels of blood, membrane, and gas at the same gas and blood velocity of 0.4 mm/s and three thicknesses of (a) 0.04 mm (b) 0.06 mm, and (c) 0.3 mm.

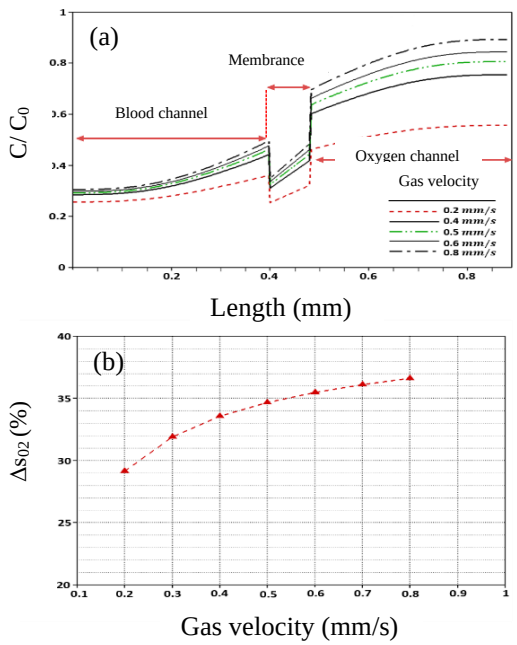

Fig. 8. (a) The oxygen concentration profile at the outlet of blood, membrane, and gas channels for the oxygen gas velocity of different inputs and (b) the percentage of oxygen diffusivity in the blood channel relative to the velocity of the various inlet gases.

Oxygen concentration profiles at various gas velocities (0.2, 0.4, 0.5, 0.6, and 0.8 mm/s) and oxygen gas diffusivity at the outlet of three gas, membrane, and blood channels are shown. A relatively good increase in oxygen diffusivity from 28% to 38% was observed with an increased gas flow rate. Of course, it should be noted that as the inlet gas velocity increases, there is no significant difference in the percent oxygen diffusion at higher velocities, only at the lowest inlet gas velocity which showed a difference of 10%.

5. Conclusions

In this study, the emission and diffusivity of gases in a microfluidic system were analyzed numerically. This study sheds light on blood and oxygen gas inlet velocity and membrane thickness as effective parameters for increasing oxygen permeability. To predict and validate the developed mathematical model, simulation results were compared with numerical and laboratory data supporting model validation. The following can be mentioned as the most significant outcomes of the present numerical solution:

The highest oxygen efficiency was observed at lower blood flow velocities (0.2 mm / s), so the oxygen diffusivity percentage reached 60%. Also, the concentration profile at the output showed qualitatively increased oxygen diffusion. Decreasing the thickness of the membrane increases the concentration gradient along the membrane, which in turn causes oxygen diffusion into the blood. Increasing the velocity of the inlet oxygen gas does not significantly affect the oxygen emission and diffusivity because we observed a maximum increase of 10%.

6. References

[1] B. Frenckner and P. Radell,“ Respiratory failure and extracorporeal membrane oxygenation”, *Semin. Pediatr. Surg.*, Vol. 17, No. 1, pp. 34-41, (2008).

[2] L. Lequier, S. B. Horton, D. M. McMullan and R. H. Bartlett,“

Extracorporeal membrane oxygenation circuitry", *Pediatr. Crit. Care Med.*, Vol. 14, No. 5_suppl, S7-S12, (2013).

[3] G. J. Peek, M. Mugford, R. Tiruvoipati, A. Wilson, E. Allen, M. M. Thalanany, C. L. Hibbert, A. Truesdale, F. Clemens and N. Cooper," Efficacy and economic assessment of conventional ventilatory support versus extracorporeal membrane oxygenation for severe adult respiratory failure (CESAR): a multicentre randomised controlled trial", *Lancet*, Vol. 374, No. 9698, pp. 1351-1363, (2009).

[4] R. R. Thiagarajan, R. P. Barbaro, P. T. Rycus, D. M. Mcmullan, S. A. Conrad, J. D. Fortenberry and M. L. Paden," Extracorporeal life support organization registry international report 2016", *ASAIO J.*, Vol. 63, No. 1, pp. 60-67, (2017).

[5] S. N. Vaslef, L. F. Mockros, R. W. Anderson and R. J. Leonard," Use of a mathematical model to predict oxygen transfer rates in hollow fiber membrane oxygenators", *ASAIO J.*, Vol. 40, No. 4, pp. 990-996, (1994).

[6] S. N. Vaslef, L. F. Mockros, K. E. Cook, R. J. Leonard, J. C. Sung and R. W. Anderson," Computer-assisted design of an implantable, intrathoracic artificial lung", *Artif. Orgns*, Vol. 18, No. 11, pp. 813-817, (1994).

[7] G. Catapano, H. D. Papenfuss, A. Wodetzki and U. Baurmeister," Mass and momentum transport in extra-luminal flow (ELF) membrane devices for blood oxygenation", *J. Membr. Sci.*, Vol. 184, No. 1, pp. 123-135, (2001).

[8] T. He, S. Yu, J. He, D. Chen, J. Li, H. Hu, X. Zhong, Y. Wang, Z. Wang and Z. Cui," Membranes for extracorporeal membrane oxygenator (ECMO): History, preparation, modification and mass transfer", *Chin. J. Chem. Eng.* , Vol. 49, No. 1, pp. 46-75, (2022).

[9] V. Evren," A numerical approach to the determination of mass transfer performances through partially wetted microporous membranes: transfer of oxygen to water", *J. Membr. Sci.*, Vol. 175, No. 1, pp. 97-110, (2000).

[10] J. Zhang, T. D. Nolan, T. Zhang, B. P. Griffith and Z. J. Wu," Characterization of membrane blood oxygenation devices using computational fluid dynamics", *J. Membr. Sci.*, Vol. 288, No. 1-2, pp. 268-279, (2007).

[11] T. Yeager and S. Roy," Evolution of gas permeable membranes for extracorporeal membrane oxygenation", *Artif. Organs*, Vol. 41, No. 8, pp. 700-709, (2017).

[12] W. J. Federspiel and K. A. Henchir," Lung, artificial: basic principles and current applications", *Biomed. Mater. Eng.*, Vol. 9, pp. 910-921, (2004).

[13] M. Dabaghi, G. Fusch, N. Saraei, N. Rochow, J. L. Brash, C. Fusch and P. Ravi Selvaganapathy," An artificial placenta type microfluidic blood oxygenator with double-sided gas transfer microchannels and its integration as a neonatal lung assist device", *Biomicrofluidics*, Vol. 12, No. 4, . 044101, (2018).

[1] M. Dabaghi, N. Saraei, G. Fusch, N. Rochow, J. L. Brash, C. Fusch and P. Ravi Selvaganapathy," An ultra-thin, all PDMS-based microfluidic lung assist device with high oxygenation capacity", *Biomicrofluidics*, Vol. 13, No. 3, . 034116, (2019).

[15] H. Matharoo, M. Dabaghi, N. Rochow, . Fusch, N. Saraei, M. Tauhiduzzaman, S. Veldhuis, J. Brash, C. Fusch, and P. R. Selvaganapathy," Steel reinforced composite silicone membranes and its integration to microfluidic oxygenators for high performance gas exchange", *Biomicrofluidics*, Vol. 12, No. 1, . 014107, (2018).

[16] N. Rochow, A. Manan, W. I. Wu, G. Fusch, S. Monkman, J. Leung, E. Chan, D. Nagpal, D. Predescu and J. Brash," An integrated array of microfluidic oxygenators as a neonatal lung assist device: in vitro characterization and in vivo demonstration", *Artif. Organs*, Vol. 38, No. 10, pp. 856-866, (2014).

[17] W. -I. Wu, N. Rochow, E. Chan, G. Fusch, A. Manan, D. Nagpal, P. R. Selvaganapathy and C. Fusch,“ Lung assist device: development of microfluidic oxygenators for preterm infants with respiratory failure”, *Lab Chip*, Vol. 13, No. 13, pp. 2641-2650, (2013).

[18] A. Gimbel, E. Flores, A. Koo, G. García-Cardeña and J. Borenstein,“ Development of a biomimetic microfluidic oxygen transfer device”, *Lab Chip*, Vol. 16, No. 17, pp. 3227-3234, (2016).

[19] J. A. Potkay,“ The promise of microfluidic artificial lungs”, *Lab Chip*, Vol. 14, No. 21, pp. 4122-4138, (2014).

[20] M. Dabaghi, N. Saraei, G. Fusch, N. Rochow, J. L. Brash, C. Fusch and P. R. Selvaganapathy,“ An ultra-thin highly flexible microfluidic device for blood oxygenation”, *Lab Chip*, Vol. 18, No. 24, pp. 3780-3789, (2018).

[21] T. Kniazeva, A. A. Epshteyn, J. C. Hsiao, E. S. Kim, V. B. Kolachalama, J. L. Charest and J. T. Borenstein,“ Performance and scaling effects in a multilayer microfluidic extracorporeal lung oxygenation device”, *Lab Chip*, Vol. 12, No. 9, pp. 1686-1695, (2012).

[22] J. A. Potkay, M. Magnetta, A. Vinson and B. Cmolik,“ Bio-inspired, efficient, artificial lung employing air as the ventilating gas”, *Lab Chip*, Vol. 11, No. 17, pp. 2901-2909, (2011).

[23] T. Rieper, C. Müller and H. Reinecke,“ Novel scalable and monolithically integrated extracorporeal gas exchange device”, *Biomed. Microdevices*, Vol. 17, No. 5, pp. 1-10, (2015).

[24] A. Thompson, L. Marks, M. Goudie, A. Rojas-Pena, H. Handa and J. Potkay,“ A small-scale, rolled-membrane microfluidic artificial lung designed towards future large area manufacturing”, *Biomicrofluidics*, Vol. 11, No. 2, . 024113, (2017).

[25] A. J. Thompson, L. J. Ma, T. J. Plegue and J. A. Potkay,“ Design analysis and optimization of a single-layer PDMS microfluidic artificial lung”, *IEEE Trans. Biomed. Eng.*, Vol. 66, No. 4, pp. 1082-1093, (2018).

[26] E. R. Weibel, *The pathway for oxygen: structure and function in the mammalian respiratory system*, 1nd ed., Harvard University Press, Cambridge, (1984).

[27] M. Dabaghi, N. Saraei, G. Fusch, N. Rochow, J. L. Brash, C. Fusch, and P. R. Selvaganapathy,“ Microfluidic blood oxygenators with integrated hollow chambers for enhanced air exchange from all four sides”, *J. Membr. Sci.*, Vol. 596, . 117741, (2020).

[28] L. J. Ma, E. A. Akor, A. J. Thompson and J. A. Potkay,“ A parametric analysis of capillary eight in single-ayer, small-scale microfluidic artificial ungs”, *Micromachines*, Vol. 13, No. 6, pp. 1-16, (2022).

[29] D. Han, A. Shah, M. A. Awad, Z. J. Wu and B. P. Griffith,“ Development of an ambulatory extracorporeal membrane oxygenation system: from concept to clinical use”, *Appl. Eng. Sci.*, Vol. 10, . 100093, (2022).

[30] S. McKee, E. A. Dougall and N. J. Mottram,“ Analytic solutions of a simple advection-diffusion model of an oxygen transfer device”, *J. Math. Ind.*, Vol. 6, No. 1, pp. 1-22, (2016).

[31] L. Mockros and R. Leonard,“ Compact cross–flow tubular oxygenators”, *ASAIO J.*, Vol. 31, No. 1, pp. 628-633, (1985).

[32] M. Shin, K. Matsuda, O. Ishii, H. Terai, M. Kaazempur-Mofrad, J. Borenstein, M. Detmar and J. P. Vacanti,“ Endothelialized networks with a vascular geometry in microfabricated poly (dimethyl siloxane)”, *Biomed. Microdevices*, Vol. 6, No. 4, pp. 269-278, (2004).

[33] J. A. Potkay,“ A simple, closed-form, mathematical model for gas exchange in microchannel artificial lungs”, *Biomed. Microdevices*, Vol. 15, No. 3, pp. 397-406, (2013).

[34] P. Puttkammer, *Boundary layer over a flat plate*, BSc report, University of Twente, Netherlands, (2013).

[35] M. S. Islam and J. Szpunar,“ Study of dialyzer membrane (polyflux 210h) and effects of different parameters on dialysis performance”, *Open J. Nephrol.*, Vol. 3, No. pp. 161-167, (2013).

[36] V. H. Huxley and H. Kutchai, “The effect of the red cell membrane and a diffusion boundary layer on the rate of oxygen uptake by human erythrocytes”, *J. Physiol.*, Vol. 316, No. 1, pp. 75-83, (1981).

[37] V. H. Huxley and H. Kutchai,“ Effect of diffusion boundary layers on the initial uptake of O2 by red cells. Theory versus experiment”, *Microvasc. Res.*, Vol. 26, No. 1, pp. 89-107, (1983).

How to cite this paper:

Behnam Dilmaghani Hassanlouei, Nader Pourmahmoud and Pierre Sullivan, “Numerical simulation of extracorporeal membrane oxygenators to investigate important parameters and membrane thickness in oxygen exchange rate,”, *J. Comput. Appl. Res. Mech. Eng.*, Vol. 13, No. 1, pp. 1-12, (2023).

DOI: 10.22061/JCARME.2023.9491.2273

URL: https://jcarme.sru.ac.ir/?_action=showPDF&article=1866